



Nanoparticle-encapsulated retinoic acid for the modulation of bone marrow hematopoietic stem cell niche

Emanuel Quartin^{a,b,1}, Susana Rosa^{a,b,1}, Sara Gonzalez-Anton^{d,e}, Laura Mosteo Lopez^{f,g,h}, Vitor Francisco^{a,b}, Delfim Duarte^{f,g,h}, Cristina Lo Celso^{d,e}, Ricardo Pires das Neves^{a,b,**}, Lino Ferreira^{a,c,*}

^a CNC—Center for Neuroscience and Cell Biology, CIBB—Centre for Innovative Biomedicine and Biotechnology, University of Coimbra, 3004-517, Coimbra, Portugal

^b IIIUC—Institute of Interdisciplinary Research, University of Coimbra, 3004-517, Coimbra, Portugal

^c Faculty of Medicine, University of Coimbra, 3004-517, Coimbra, Portugal

^d Department of Life Sciences, Imperial College London, South Kensington Campus, The Francis Crick Institute, London, UK

^e Haematopoietic Stem Cell Laboratory, The Francis Crick Institute, London, UK

^f Instituto de Investigação e Inovação em Saúde (i3S), University of Porto, Porto, Portugal

^g Department of Biomedicine, Faculdade de Medicina da Universidade do Porto (FMUP), Porto, Portugal

^h Department of Onco-Hematology, Instituto Português de Oncologia (IPO)-Porto, Porto, Portugal

ARTICLE INFO

Keywords:

Light
Nanoparticles
Retinoic acid
Leukemia
M1 macrophages
Drug delivery

ABSTRACT

More effective approaches are needed in the treatment of blood cancers, in particular acute myeloid leukemia (AML), that are able to eliminate resistant leukemia stem cells (LSCs) at the bone marrow (BM), after a chemotherapy session, and then enhance hematopoietic stem cell (HSC) engraftment for the re-establishment of the HSC compartment. Here, we investigate whether light-activatable nanoparticles (NPs) encapsulating all-trans-retinoic acid (RA⁺NPs) could solve both problems. Our *in vitro* results show that mouse AML cells transfected with RA⁺NPs differentiate towards antitumoral M1 macrophages through RIG.1 and OASL gene expression. Our *in vivo* results further show that mouse AML cells transfected with RA⁺NPs home at the BM after transplantation in an AML mouse model. The photo-disassembly of the NPs within the grafted cells by a blue laser enables their differentiation towards a macrophage lineage. This macrophage activation seems to have systemic anti-leukemic effect within the BM, with a significant reduction of leukemic cells in all BM compartments, of animals treated with RA⁺NPs, when compared with animals treated with empty NPs. In a separate group of experiments, we show for the first time that normal HSCs transfected with RA⁺NPs show superior engraftment at the BM niche than cells without treatment or treated with empty NPs. This is the first time that the activity of RA is tested in terms of long-term hematopoietic reconstitution after transplant using an *in situ* activation approach without any exogenous priming or genetic conditioning of the transplanted cells. Overall, the approach documented here has the potential to improve consolidation therapy in AML since it allows a dual intervention in the BM niche: to tackle resistant leukemia and improve HSC engraftment at the same time.

1. Introduction

Acute myeloid leukemia (AML) is a heterogenous group of blood

cancers characterized by rapid proliferation and arrested differentiation of transformed hematopoietic progenitors, resulting in the accumulation of immature myeloid precursors in the bone marrow (BM) and

Peer review under responsibility of KeAi Communications Co., Ltd.

* Corresponding author. CNC—Center for Neuroscience and Cell Biology, CIBB—Centre for Innovative Biomedicine and Biotechnology, University of Coimbra, 3004-517, Coimbra, Portugal.

** Corresponding author. IIIUC—Institute of Interdisciplinary Research, University of Coimbra, 3004-517, Coimbra, Portugal.

E-mail addresses: emanuelquartin@gmail.com (E. Quartin), susrosa@gmail.com (S. Rosa), s.gonzalez-anton@imperial.ac.uk (S. Gonzalez-Anton), laura.mosteo@ibmc.up.pt (L. Mosteo Lopez), francisco.vms@gmail.com (V. Francisco), delfimd@med.up.pt (D. Duarte), c.lo-celso@imperial.ac.uk (C. Lo Celso), ricardo.neves@uc-biotech.pt, r.neves@cnc.uc.pt (R. Pires das Neves), lino.ferreira@uc.pt, lino@uc-biotech.pt (L. Ferreira).

¹ Equal contribution.

<https://doi.org/10.1016/j.bioactmat.2023.12.017>

Received 8 July 2023; Received in revised form 16 December 2023; Accepted 21 December 2023

2452-199X/© 2023 The Authors. Publishing services by Elsevier B.V. on behalf of KeAi Communications Co. Ltd. This is an open access article under the CC BY-NC-ND license (<http://creativecommons.org/licenses/by-nc-nd/4.0/>).

peripheral blood [1,2]. This uncontrolled expansion of malignant hematopoietic precursor cells occurs at the expense of normal hematopoietic cells and results in the exhaustion of the BM. Standard AML therapies include induction chemotherapy followed by consolidation with chemotherapy and allogeneic HSC transplantation [1]. Sixty percent of adult patients with ages below 60 years are not cured by conventional therapies [1]. A particular subtype of AML, the acute promyelocytic leukemia (APL) is a paradigm of therapy success [3]. Treatment of APL patients with all-trans-retinoic acid (RA) and arsenic trioxide induces the differentiation of malignant promyelocytes and leads to cure rates of 90% [4]. On the other hand, the limited efficacy of the conventional treatments in other subtypes of AML may be ascribed to several reasons including (i) the resistance of leukemia stem cells (LSCs) that reside in microenvironmental niches in the bone marrow that are difficult to access by therapeutic interventions [5] and (ii) low efficiency of HSC engraftment after transplantation [1]. Several pre-clinical strategies have been tested to tackle this, including manipulation of the LSC niche [6] and *ex vivo* treatment of stem cells with pro-survival/pro-engraftment factors [7–9]; however, with limited efficacy.

RA is a small molecule with bipolar effects in HSCs. RA has very low solubility in aqueous solution (μM range at pH 7.3) [10] and thus requires specific binding proteins such as CRABPs to be transported within cells to act at nuclear receptors. In addition, RA is rapidly (few hours) degraded after systemic administration by the cytochrome P450-dependent monooxygenase system [11]. Importantly, RA may contribute for the differentiation of hematopoietic stem cells [12] as well as their engraftment at the BM [13], by the activation of nuclear RA receptors (RARs). Thus, approaches to deliver controlled amounts of RA inside the bone-marrow niches may be an elegant strategy to modulate the activity of non-diseased and/or malignant hematopoietic cells.

NPs may be an approach to deliver RA within the BM, in particular to the HSC niche. The HSC niche is formed by HSCs and support cells such as perivascular mesenchymal stem cells, endothelial cells, megakaryocytes, macrophages, neurons, among others [14,15]. HSCs have the capacity to self-renew and recapitulate the entire blood system hierarchy upon serial transplantation. The classical view is that HSCs can be divided into two subpopulations according to their CD34 expression: CD34⁺ long-term (LT)-HSCs and CD34⁺ short-term (ST)-HSCs [16,17]. LT-HSCs are a rare, quiescent population in bone marrow and have full long-term (>3–4 months) reconstitution capacity, whereas ST-HSCs only have a short-term (mostly <1 month) reconstitution ability. LT-HSCs differentiate into ST-HSCs, and subsequently, ST-HSCs differentiate into multipotent progenitors (MPPs), which have no detectable self-renewal ability and generate lineage-restricted progenitors, and finally, mature effector cells [16]. We now know that this classical model oversimplifies the complexity of hematopoietic stem and progenitor cells (HSPCs) as it is based on surface markers and transplantation using bulk cells. Recent advances in single cell technology and genetic mouse models have identified new types of HSPCs with different lineage biases. In the last few years, a new term was coined-dormant HSCs-that was shown to be dependent on RA signaling [13].

Lipid-polymer NPs [18] or polymeric NPs [19] have been reported to target BM niche and deliver drugs such as siRNAs [18] and small molecules [19] (e.g. Bortezomib, an anti-cancer medication used to treat multiple myeloma and mantle cell lymphoma). Moreover, several NP formulations (none for RA release) have been developed to target leukemic cells in the BM niche based on NPs conjugated with E-selectin thioaptamer [20], CD45.2 antibody [21] or CD117 antibody [22]. However, all these formulations have limitations because although they target the BM, they still accumulate in other regions of the body and thus may lead to toxic effects. Several NP formulations have been reported in the last 15–20 years for the delivery of RA based in the complexation of the RA with proteins or cationic polymers, by physical encapsulation in polymeric or inorganic nanoparticles, microparticles, micelles,

liposomes, among others [3]. Yet these formulations have limitations since they do not target the BM. Recently, we have tested an alternative strategy based on the use of hematopoietic cells to transport light-triggerable RA-containing NPs to the BM niche [6]. We have used light-triggerable NPs to prevent the premature release of RA from the formulation which could induce a differentiation process of the transporting cell and thus the loss of cell tropism to the BM. When the NPs were activated by a blue laser, the disassembly of the NPs promoted a biological differentiation program in the transporting cells which in turn lead to the differentiation of leukemia cells at the HSC niche. However, it remained to be determined the impact of the formulation in the *in vivo* differentiation of the transporting cells as well as the resident diseased hematopoietic cells, both locally (at the site of light activation in calvaria BM) and systemically (e.g. long bones) as well as the effect of the formulation in biological processes mediated by non-diseased hematopoietic cells, in particular, its potential to engraft transplanted HSCs.

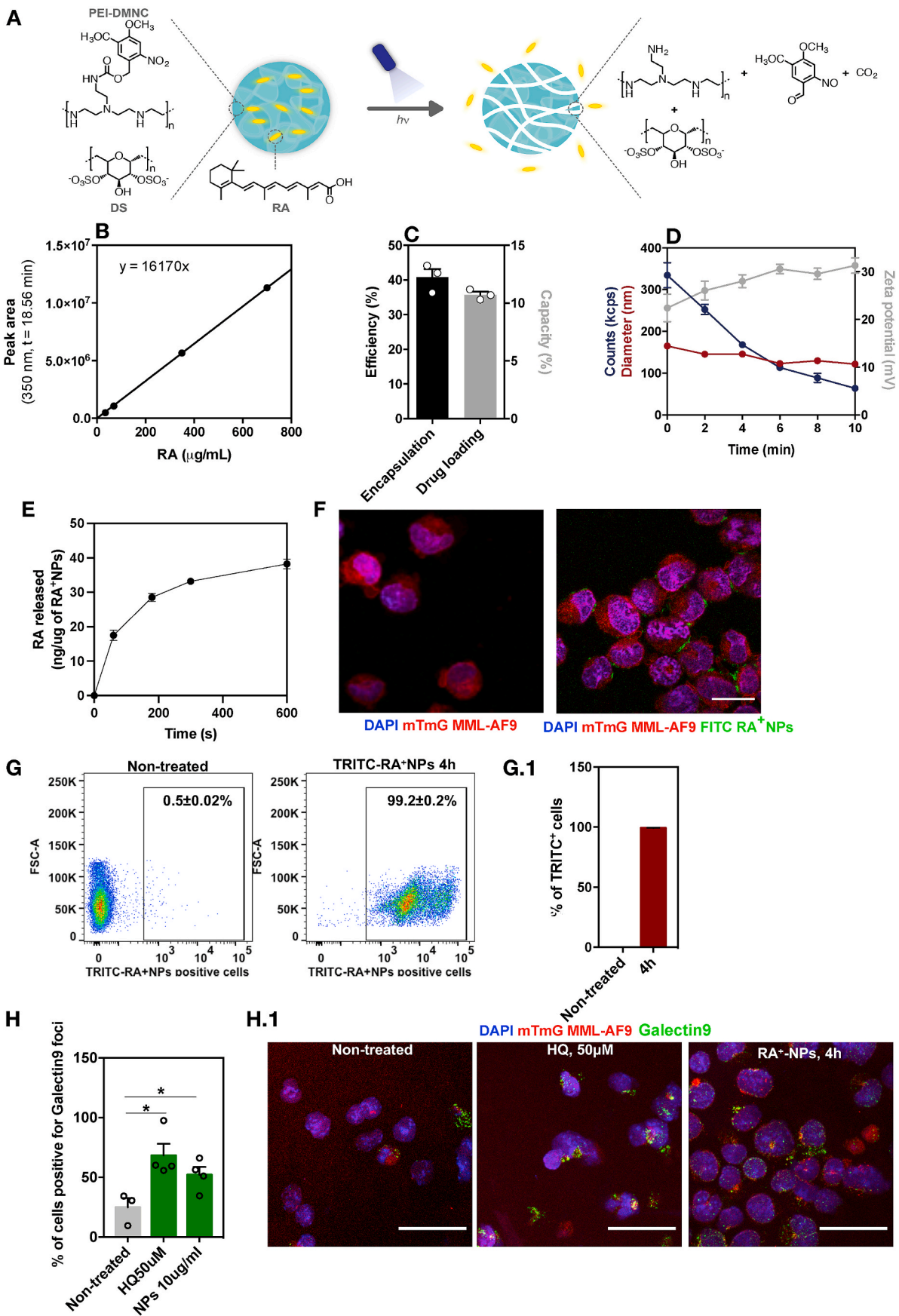
Here, we have investigated the impact of the delivery of light-triggerable NPs by hematopoietic cells in two different settings: (i) to modulate the diseased HSC BM niche in an AML mouse model and (ii) to enhance HSC engraftment in the BM niche. Initially, we have investigated whether RA-containing NPs (RA⁺NPs) could modulate the differentiation program of leukemic blasts, how different was that effect compared to soluble RA and the mechanisms governing the differentiation program. Then, we have studied the *in vivo* differentiation program of leukemia cells transfected with RA⁺NPs and their impact in the overall number of leukemia cells at different BM sites. Finally, we evaluated the impact of RA⁺NPs in the engraftment of healthy HSCs (Lineage^cKit⁺ cells) in the BM.

2. Results and discussion

2.1. *In vitro* effect of RA⁺NPs in mouse AML cells

Light-inducible polymeric NPs were prepared according to a previous study reported by us [6]. Poly(ethyleneimine) (PEI) was initially derivatized with 4,5-dimethoxy-2-nitrobenzyl chloroformate (DMNC), a light-sensitive photochrome (Fig. 1A). Then, RA was mixed with PEI-DMNC to form complexes through the electrostatic interactions of the carboxyl groups of RA with the amine groups of PEI. The formation of a complex between RA and PEI has been previously demonstrated [23]. A solution of RA with PEI-DMNC was then added to dextran sulfate (DS) to form NPs (RA⁺NPs) by electrostatic and hydrophobic interactions. To stabilize the NP formulation, zinc sulfate was added. The resultant NP formulation contained approximately 110 μg of RA per mg of NP, an average diameter of 165 nm and a zeta potential of 22 mV (Fig. 1B and D) like what was previously described by us. The loading efficiency and encapsulation efficiency of RA was $10.7 \pm 0.2\%$ and $40.8 \pm 2.3\%$ respectively (Fig. 1C). Once these RA⁺NPs are exposed to blue light they photo-disassembled, releasing the RA from their core (Fig. 1D). Approximately 35 ng of RA was released per μg of NP after 5 min of blue light activation (Fig. 1E).

Initially, we investigated whether AML cells could internalize RA⁺NPs. Both *in vitro* and *in vivo* biosafety profiles of these RA⁺NPs have been previously reported by us in different contexts [6,24]. For this purpose, we used a murine non-APL AML disease model which encompasses the fusion oncogene MLL-AF9. In this model, most of the leukemia stem cells (LSCs) are phenotypically similar to granulocyte-macrophage progenitor (GMP) cells [25] but they are sensitive to RA-induced upregulation of myeloid differentiation genes [26]. Our results show that cells were able to internalize RA⁺NPs (Fig. 1F, G and G.1) without inducing a measurable cytotoxic program (Supplementary Fig. 1B and B.1). Effective RA intracellular delivery requires not only that the nanoformulation is taken up by the cells, but it also escapes the endosomal compartment and releases its cargo to the cytosol. To determine the capacity of RA⁺NPs to escape the endosomal



(caption on next page)

Fig. 1. Physicochemical characterization of RA⁺NPs and internalization in MML-AF9 cells. (A) Schematic representation of RA⁺NP synthesis and photo-disassembly. (B) Calibration curve for HPLC quantification of RA in the NPs. (C) Percentage of encapsulation efficiency and drug loading capacity of RA in the NPs. (D) Number of NPs (kcps), size and zeta potential of an aqueous suspension of RA⁺NPs (50 µg/mL) exposed to UV lamp (365 nm, 100 W) for up to 10 min. In C and D, values are the Mean ± SEM (n = 3). (E) Release profile of [³H]-RA from light-activatable NPs (10 µg/mL in water) after exposure to a blue laser (405 nm, 80 mW/cm²). (F) Representative confocal images of tomato fluorescent (mTmG) MML-AF9 cells with and without a 4 h incubation with FITC-labelled RA⁺NPs (10 µg/mL) for 4 h. Scale bar is 20 µm. (G) Representative flow cytometry plots of the internalization of TRITC RA⁺-NPs (10 µg/mL, 4 h) in yellow fluorescent (YFP) MML-AF9 cells. (G.1) Quantification of the internalization of TRITC RA⁺-NPs in YFP MML-AF9 cells. The values are the mean ± SEM (n = 3). (H) Percentage of cells positive for galectin 9 foci in mTmG MML-AF9 cells either treated with RA⁺-NPs (10 µg/mL) or hydroxychloroquine (HQ, 50 µM) for 4 h in serum-free RPMI-1640 or non-treated. After an additional 24 h period in complete RPMI-1640 the cells were fixed and immunostained. Values are the Mean ± SEM (n = 4). (H.1) Representative confocal images of galectin 9 staining (green) of mTmG MML-AF9 cells (red). Scale bar is 50 µm. Statistical analyses were performed by a Students *t*-test. *P < 0.05.

compartment, we monitored the induction of galectin 9 foci after NP internalization (Fig. 1H and H.1). This protein has been used to monitor endolysosomal compartment disruption [27]. Cells treated with RA⁺NPs showed an increased number of galectin 9 foci compared to non-treated cells. The level of galectin 9 expression was comparable to the one observed with hydroxychloroquine, which was used as positive control, indicating that RA⁺NPs escaped from the endosomal compartment within 24 h after transfection.

Next, we investigated whether RA⁺NPs could modulate the differentiation program of MLL-AF9 blasts. Cells were transfected for 4 h with RA⁺NPs (10 µg/mL of NPs containing 1.1 µg/mL of RA), washed, activated for 5 min with a blue laser (405 nm, 80 mW) and allowed to differentiate for 3 days followed by flow cytometry characterization (Fig. 2 and Supplementary Fig. 1A). Under these laser treatment conditions, there was no significant impact in cell viability in comparison with non-treated cells (Supplementary Fig. 1B and B.1). As controls, MLL-AF9 cells were cultured in medium supplemented with RA (1.1 µg/mL of RA) for 3 days or empty NPs (i.e. without RA; activated with the blue laser). As expected, the differentiation profile of cells treated with empty NPs was like the non-treated condition (data not shown). Interestingly, soluble RA and RA delivered by NP activation seem to promote distinct differentiation pathways in MLL-AF9 cells (Fig. 2C). RA⁺NPs induce higher differentiation of MLL-AF9 blasts into monocyte/macrophage (CD11b⁺Ly6G⁻ F4/80⁺) than soluble RA (Fig. 2C and D). In contrast, soluble RA was able to induce higher differentiation of MLL-AF9 blasts towards granulocyte lineage, more specifically towards neutrophil-like cells (CD11b⁺Ly6G⁺), as previously reported [26], than RA⁺NPs (Fig. 2B and C). Although previous studies have shown that AML cells can differentiate towards monocyte/macrophage lineage *in vitro* when treated with vitamin D [28], which can be further enhanced by combining vitamin D treatment with RA, this is the first time to our knowledge that monocyte/macrophage differentiation is observed with RA treatment alone. Furthermore, activation of RA⁺NPs seems to promote type 1 macrophage polarization (M1) (MHC II⁺CD206⁻) which has been shown to suppress tumor growth [29], in contrast to type 2 macrophages (M2) (Fig. 2D). Importantly, it has been shown in the MLL-AF9 leukemia mouse model the presence of similar levels of M1 versus M2 macrophages in the spleen and BM reservoirs and repolarizing these cells to the M1 phenotype by a pharmacological agent (not RA) was important to tackle leukemia in the animal model [30].

Altogether, our results indicate that RA⁺NPs are internalized by AML cells, able to escape the endolysosomal compartment and induce higher differentiation of AML blasts into monocyte/macrophage than soluble RA. In addition, RA⁺NPs induce higher polarization of macrophages into M1 phenotype than soluble RA.

2.2. Potential mechanisms behind the bioactivity of RA⁺NPs vs soluble RA in AML cells

RA concentration and presentation (i.e., with or without membrane-receptor signaling) may account for the differences found in the differentiation program of AML cells exposed to RA⁺NPs or soluble RA. It is possible that the increase observed in monocyte/macrophage differentiation is due to particularly high concentrations of RA being delivered

inside the cell. To have more mechanistic information, we conducted mRNA expression analyses in MLL-AF9 cells treated with soluble RA (0.11 µg/mL) or RA⁺NPs (1 µg/mL of RA⁺NPs containing 0.11 µg/mL of RA). In this experiment, we have decreased the concentration of RA⁺NPs and soluble RA to have high sensitivity to measure its molecular impact. As the transcriptional events related with monocyte-to-macrophage differentiation and subsequent M1 or M2 cell polarization induced by RA are largely unexplored we focused our analyses on specific genes previously described to show major changes in M-CSF dependent differentiation in response to LPS plus IFN-γ or IL-4 [31] and on a recent report on single-cell transcriptomics of monocyte/macrophage phenotypes in the acute myeloid leukemia microenvironment [32]. Our results show that RA⁺NPs can induce stronger up-regulation of specific monocyte/macrophage genes than soluble RA (Fig. 3A). RA⁺NPs induce an early (24 h) increase in both CEBP-alpha and PU.1 genes that are important for both granulocyte and monocyte differentiation; however, at 72 h after treatment there is a drop in CEBP-alpha but PU.1 remains high, this correlates well with the commitment to the monocyte lineage instead of the granulocyte fate [26,33]. Also, the expression of Ly6G is highly induced in the soluble RA treatment indicative of granulocyte lineage commitment while in the RA⁺NP treatment after an early increase the expression drops at 72 h. This result mimics what happens in the bone marrow where monocytes express Ly6G transiently during bone marrow development, while Ly6G expression in granulocytes and peripheral neutrophils directly correlates with the level of differentiation and maturation. Also, the drop in Ly6E after soluble RA treatment indicates granulocyte commitment in comparison with Ly6E expression maintenance in monocytes [34]. The monocyte to macrophage differentiation can be seen in the increased expression of the MHC II gene H2DMB2 after 72 h. Moreover, these cells showed a significant increase in the expression of genes characteristic of early signaling pathways (24 h) in macrophage differentiation like CSF1R and CX3CR1 (Fig. 3B). On the other hand, there is a drop in the expression of CD206 that was implicated in an immunosuppressive M2-like pro-leukemic phenotype [35,36]. These results together with the increased expression of CD80, CD86, IL2RA and the cytokines/chemokines TNF-α, CXCL10, IL1-β and IL12A, known markers of M1 polarization [37–39], suggest that RA⁺NPs induced the differentiation of MLL-AF9 cells towards an M1-like phenotype (Fig. 3C).

Several kinase signaling pathways important in the context of differentiation induced by RA have been studied [40,41] (Fig. 3D). Our results showed that MLL-AF9 cells treated with RA⁺NPs showed higher expression of P38, PKA, MSK1, and ERK1, when compared with cells treated with soluble RA (Fig. 3D). RIG-1 has been repeatedly described as a cytoplasmic RNA receptor that plays a vital role in the innate antiviral immunity together with 2'-5' oligoadenylate like protein (OASL), a protein that belongs to a well-known family of antiviral proteins. It has been recently highlighted that RIG-1 is important for myeloid differentiation [42]. While RA by itself can induce RIG-1 and promote myeloid differentiation it is not able to maintain activation of OASL (besides 24 h) and in this way potentiate RIG-1 signaling over the time. On the contrary, RA⁺NPs seem to induce a similar RIG-1 response in the first 24 h but as OASL is induced at later times. This tendency was also observed when OASL and RIG-1 protein levels were monitored

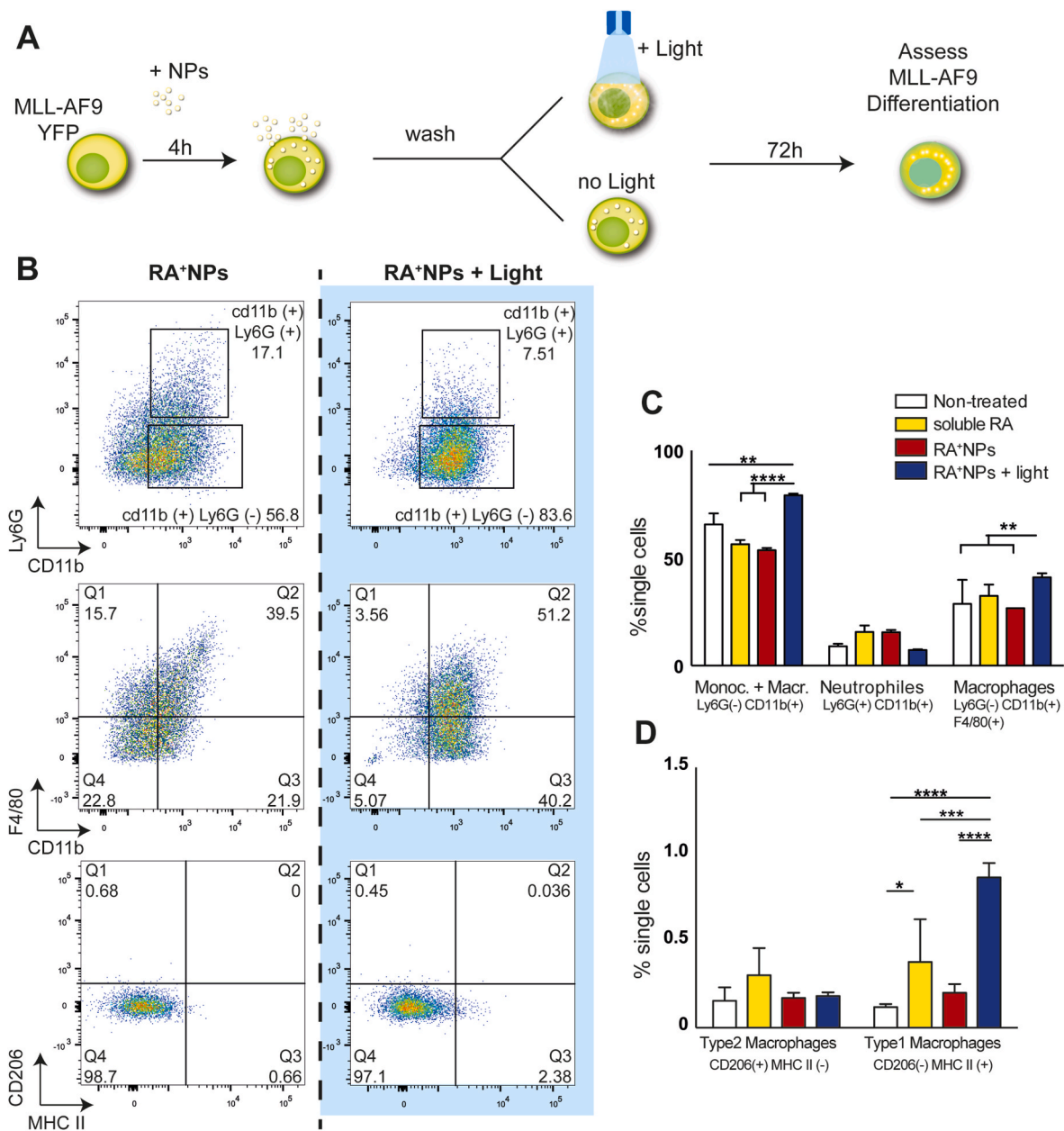


Fig. 2. Intracellular delivery of RA⁺NPs promotes monocyte/macrophage differentiation of murine AML blasts. (A) Schematic representation of the experiment. MLL-AF9 YFP cells were incubated in serum-free medium with RA⁺NPs (10 μg/mL) for 4 h. Then, cells were washed three times with PBS to remove NPs not internalized, activated or not by blue laser (405 nm, 80 mW, 5 min) and finally cultured in complete medium for additional 3 days. Alternatively, MLL-AF9 YFP were cultured in complete medium for 3 days having soluble RA (1.1 μg/mL). (B) Representative gating strategy for Lin⁻ MLL-AF9 YFP cells treated with RA⁺NPs. Dead cells were excluded by DAPI staining. Percentages of cells in each quadrant are relative to the previous gated population. (C) Percentage of cells expressing monocyte (Ly6G⁻CD11b⁺), neutrophil (Ly6G⁺CD11b⁺) and macrophage (Ly6G⁻CD11b⁺F4/80⁺) differentiation markers. (D) Percentage of cells expressing macrophage activation markers for type 1 (MHC II⁺CD206⁻) and type 2 (MHC II⁻CD206⁺). (C–D) Bars reflect the percentages of positive cells with respect to the initial gating for the population of live and single cells and were calculated based on the isotype controls. In C and D results are expressed as Mean ± SEM (n = 3). Statistical analyses were performed by two-way ANOVA followed by a Holm-Sidak post-test. *P < 0.05, **P < 0.01, ***P < 0.001 and ****P < 0.0001.

(Supplementary Fig. 2). Therefore, the RIG-1/OASL complex may remain active more time and, in this way, have an impact in macrophage differentiation/activation (Fig. 3D and E). As OASL is considered a type I interferon signature gene [43,44] this may be the reason for a shift towards the M1 macrophage fate when RA was delivered through the NP system (Fig. 3E). Further tests should be done in the near future to clarify this issue.

Overall, our *in vitro* experiments indicate that the encapsulation of RA in NPs constitutes an effective way to direct MLL-AF9 cells towards an anti-tumoral macrophage phenotype.

2.3. Mouse AML cells transfected with RA⁺NPs significantly decrease the leukemia levels at the bone marrow in an AML mouse model

To evaluate *in vivo* the therapeutic potential of RA⁺NPs, mouse AML cells were transfected with the formulation, transplanted in an AML mouse model and the leukemia levels monitored at the BM. First tomato fluorescent mTmG MLL-AF9 blasts were injected in healthy mice to induce disease infiltration (Fig. 4A). After 11 days, yellow fluorescent YFP MLL-AF9 blasts previously loaded with RA⁺NPs or empty NPs were injected. Twenty-four hours later (day 1), intravital microscopy [45] was used to confirm the homing of YFP blasts to the same niche as

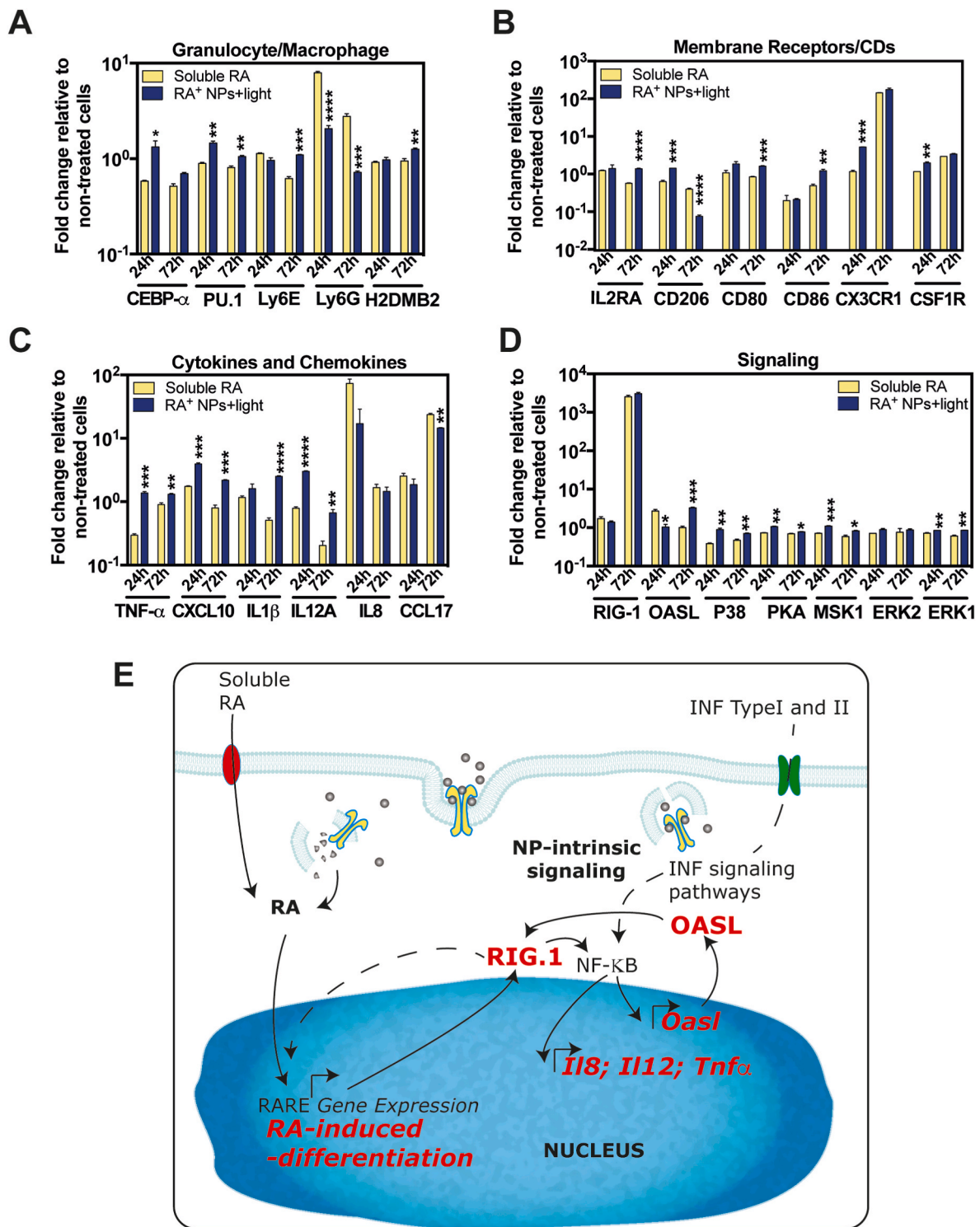


Fig. 3. Transcriptional changes induced by RA in murine AML blasts are dependent on the delivery approach. (A–C) mRNA expression profile induced by soluble RA or RA⁺NPs at 24 h and 72 h. (D) mRNA expression profile induced by soluble RA or RA⁺NPs in terms of signaling pathways involved in macrophage differentiation. (E) Schematic representation of RA signaling highlighting a possible mechanism for the co-adjuvant activity intrinsic to the NP. In A, B, C and D, the values are Mean ± SEM (n = 3). The mRNA levels were normalized by the housekeeping gene GAPDH and represented as fold increase or decrease relative to the respective untreated control. Statistical analyses were performed by a Students *t*-test. *P < 0.05, **P < 0.01, ***P < 0.001 and ****P < 0.0001.

mTmG blasts (Supplementary Fig. 3), and NPs were activated by exposing the mouse calvaria to the blue laser for 10 min. This activation was repeated the following day. Three days after the last activation (i.e. day 5 after cell transplantation), the progression of the disease and MLL-AF9 activity were monitored inside the niche by time-lapse image acquisition (Fig. 4). At the end of the acquisitions, mice were sacrificed,

and BM was collected from the calvaria and long bones and analyzed by flow cytometry (Fig. 5). Image analysis showed a reduction of mTmG blasts inside the calvaria BM niche in mice that received YFP MLL-AF9 blasts transfected with RA⁺NPs relatively to mice that received YFP MLL-AF9 blasts transfected with empty NPs (Fig. 4B and C). Flow cytometry results showed that mice treated with YFP MLL-AF9 blasts

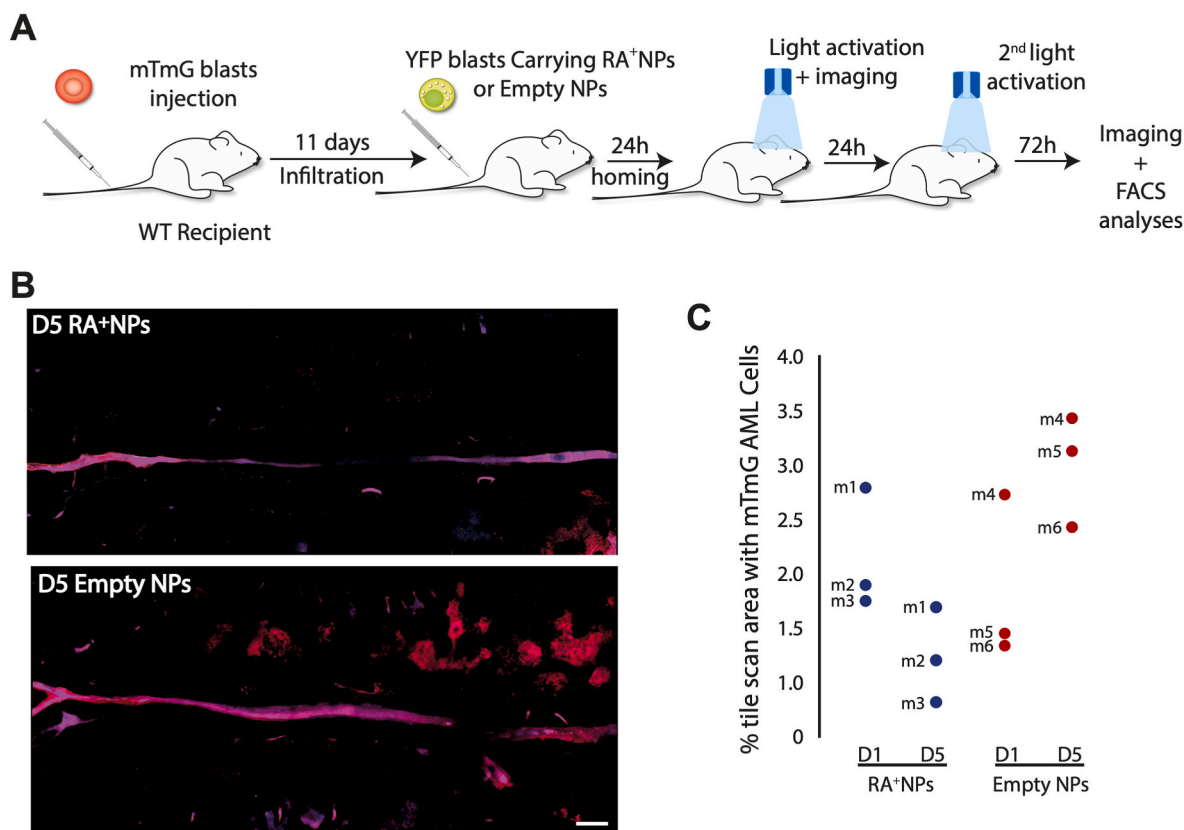


Fig. 4. RA⁺NPs prevent leukemia progression *in vivo*. (A) Schematic representation of the protocol for the generation of murine MLL-AF9 mTmG AML disease model. 100,000 primary mTmG AML blasts were transplanted by tail vein injection into non-irradiated secondary recipients. In all secondary recipients, progressive blast expansion was observed at day 11 post-transplantation. At this stage 1 million YFP MLL-AF9 blasts previously loaded with RA⁺NPs or empty NPs were tail vein injected into these mice. After 24 h, homing was confirmed by tilescan imaging of the calvaria bone, and blue light activation was performed (80 mW, 5 min) and repeated on the next day. On day 5, disease progression was assessed by tilescan imaging followed by FACS analyses of the calvaria and long bones BM. (B) Representative tilescans of day 5 calvaria BM of mice treated with YFP⁺ MLL-AF9 blasts loaded with RA⁺ NPs or Empty NPs. MLL-AF9 colonies can be seen in red while the main central blood vessels are blue. (C) Graph showing the percentage of mTmG cells present in the calvaria of each mouse at days 1 and 5. Disease progression was monitored by quantifying the area occupied by mTmG cells at days 1 and 5 with respect to the total imaged area (approximately 6.5 mm²).

transfected with RA⁺NP had reduced mTmG MLL-AF9 blast infiltration in the BM, both in the calvaria (the site of activation; local effect) and in the long bones (Fig. 5), which is indicative of a systemic effect of the treatment. YFP MLL-AF9 blasts transfected with RA⁺NP showed higher, although not statistically different, monocyte and macrophage differentiation in both BM sites in animals treated with RA⁺NPs relatively to the ones treated with cells transfected with empty NPs (Fig. 5E). Moreover, when the healthy BM population was assessed in terms of differentiation profile it was also evident that RA⁺NPs induce a similar effect in the long bones.

Overall, our results showed that YFP MLL-AF9 blasts transfected with RA⁺NP and transplanted in an AML mouse model significantly decreased the number of mTmG blasts both in the site of irradiation as well as in other BM locations. This unexpected result suggests a crosstalk between the treatment site and other BM niches. In addition, our results show that the transfected cells (YFP⁺ cells) have more propensity to differentiate into macrophages and monocytes than cells transfected with empty NPs.

2.4. *In vitro* effect of RA⁺NPs on hematopoietic progenitor cells (CD34⁺ cells): cytotoxicity, internalization kinetics and cell differentiation program

The standard consolidation therapy in AML includes conventional chemotherapy and allogeneic HSC transplantation alone or most commonly in combination [1]. To potentiate the engraftment of HSCs we have tested the concept of transfecting the cells with RA⁺NPs and activate the NPs after cell homing in the BM. Initially, we investigated by

flow cytometry the impact of RA⁺NPs in human umbilical cord blood (UCB) CD34⁺ cells, a common cell source used in hematopoietic stem cell transplantation (HSCT). As the laser exposure may have high impact in cell viability, different laser powers were tested (Fig. 6A). Laser powers higher than 20 mW for 5 min had a significant effect in cell viability. Yet, a laser power of 40 mW for 1 min had no measurable cytotoxicity (Fig. 6B, Supplementary Fig. 4A). Finally, we tested the combined effect of the laser exposure and NP treatment in UCB CD34⁺ cells (Fig. 6C, Supplementary Fig. 4B). Although the laser exposure still seems to have a negative effect in terms of viability in cells without NP treatment, the toxicity effect is decreased with increased concentrations of NP treatment. In fact, no significant toxicity is observed in cells treated with 10 µg/mL NPs with or without subsequent laser exposure for 60 s at 40 mW laser power. This could be due to the capacity of the NPs to absorb the irradiation due to the presence of the light-sensitive photochrome DMNC.

Next, we characterized the internalization kinetics and the dilution of internalized NPs during extended cell culture periods (Fig. 6D–F). Cells were treated with TRITC-labelled RA⁺NPs for different periods of time, washed to remove the non-internalized NPs, and NP internalization levels assessed by flow cytometry. Approximately 100% of CD34⁺ cells were labelled with TRITC-labelled RA⁺NPs in 4 h (Fig. 6E). Confocal microscopy studies confirmed the internalization of NPs and showed that NPs were not distributed homogeneously in the cell cytoplasm, showing some polarization (Fig. 6G).

To understand whether these cells lose these NPs after some time, the cells were cultured for an additional 3 or 6 days. At the selected time

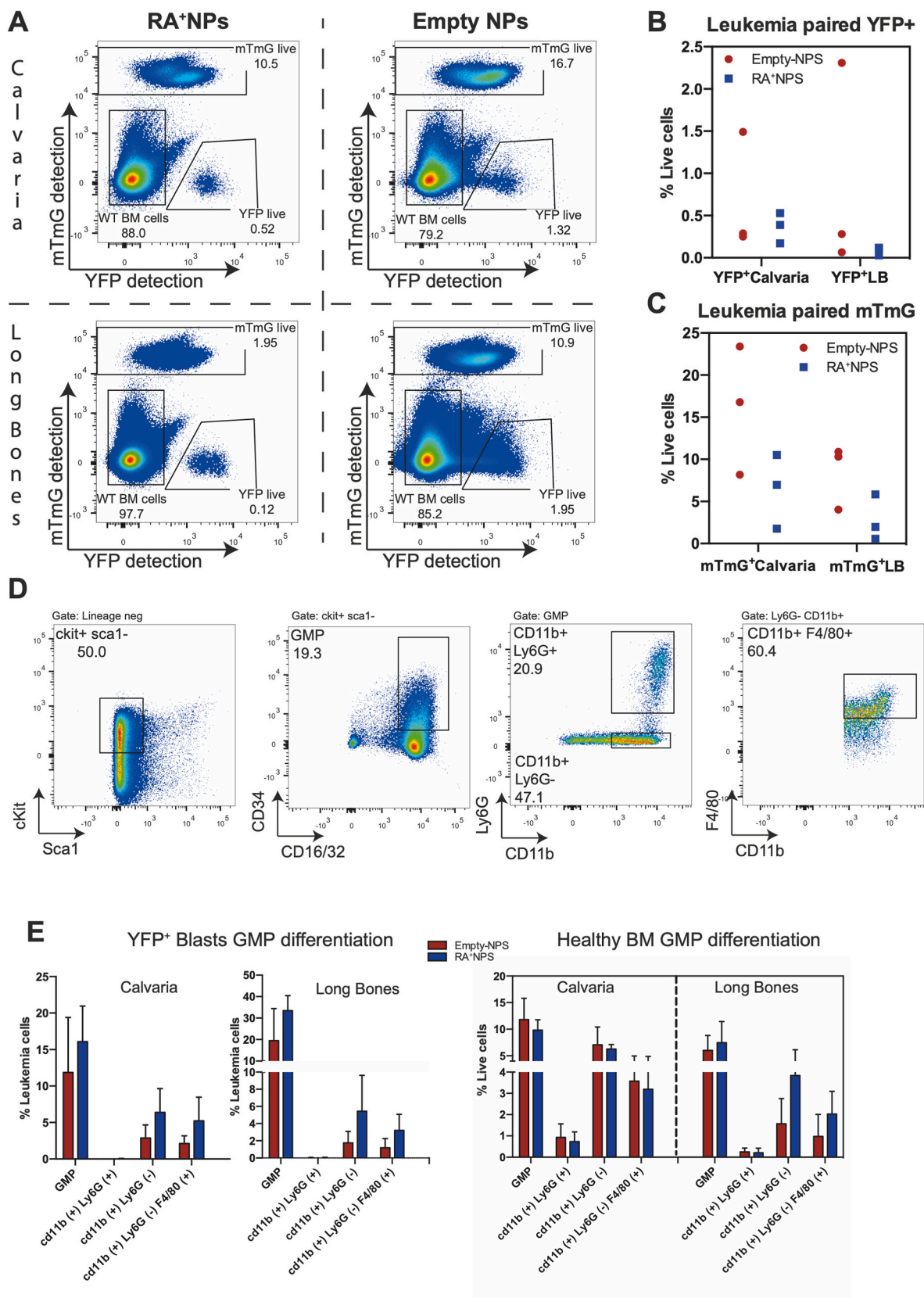


Fig. 5. *In vivo* activation of RA⁺ NPs promotes differentiation of delivery cells and resident healthy BM cells. (A) Representative plots of flow cytometry gating strategy analysis for quantification of MLL-AF9 YFP and mTmG cells at calvaria and long bone BM. Mice were treated in pairs with empty or RA⁺ NPs (n = 3). (B, C) Treatment with YFP MLL-AF9 RA⁺ NPs, induces a decrease in both delivery and resident leukemia cell numbers when compared with mice treated with empty NPs. (D) Phenotypic analyses of myeloid differentiation were performed by gating GMPs (Lin⁻ cKit⁺, Sca1⁻ CD34⁺ CD16/32⁺) and evaluating the expression levels of Ly6G, CD11b and F4/80 in the BM of calvaria and long bones. (E) Myeloid differentiation levels of MLL-AF9 blasts and non-disease BM cell population at the calvaria and long bones. Results are expressed as Mean ± SEM (n = 3).

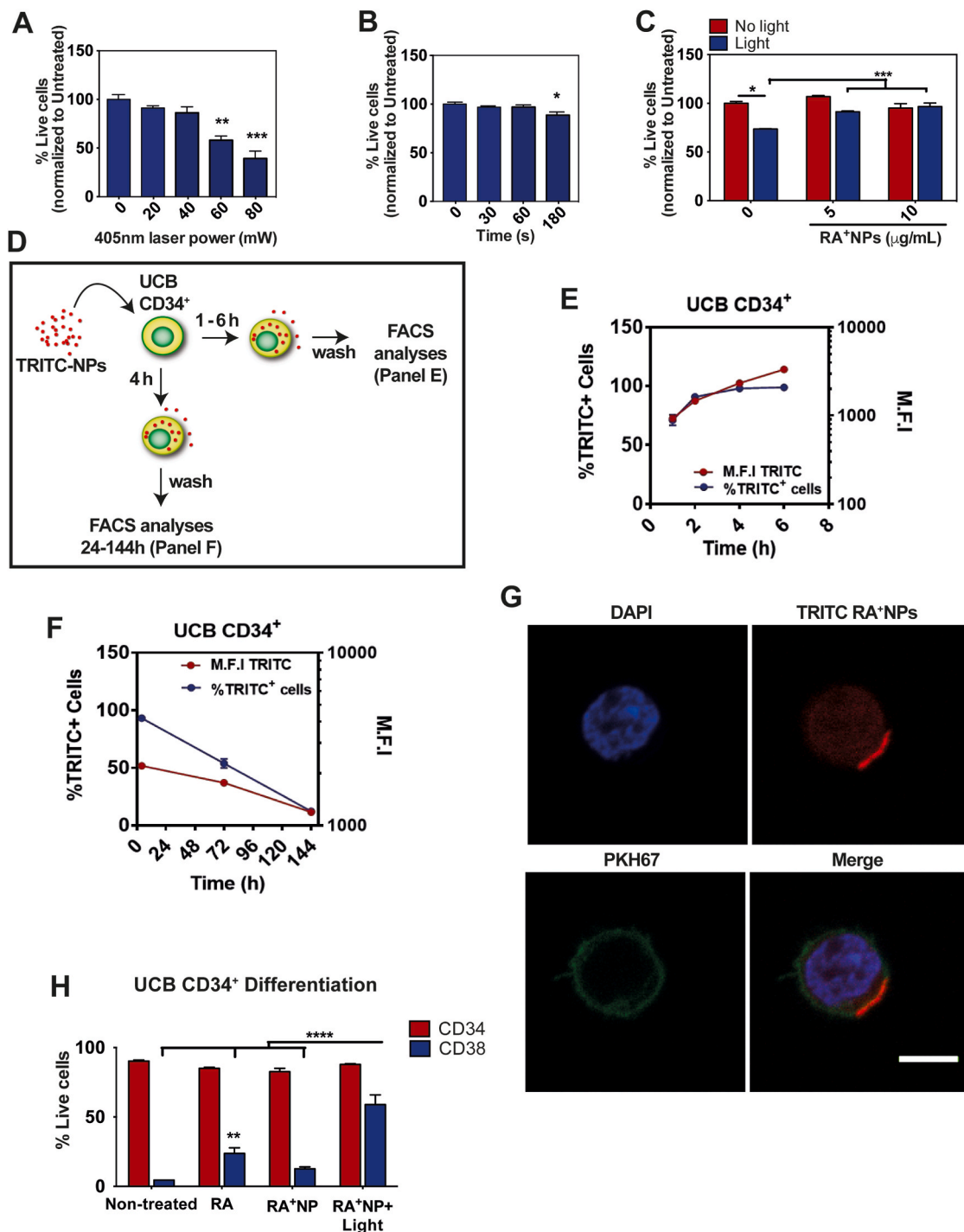


Fig. 6. Biocompatibility, internalization kinetics and bioactivity of light-activated RA⁺NPs in human UCB CD34⁺ cells. (A–C) Cytotoxicity of RA⁺NPs and laser exposure were tested in human UCB CD34⁺ cells 48 h post-treatment by Annexin/PI staining followed by flow cytometry analysis. Live cells were negative for Annexin V and PI staining. (A) Percentage of live cells exposed to a blue laser for 5 min at different laser powers. (B) Percentage of live cells exposed to a blue laser at 40 mW for different time periods. (C) Percentage of live cells cultured in medium supplemented with different concentrations of RA⁺NPs for 4 h, washed and exposed or not to a blue laser (1 min, 405 nm, 40 mW). (D) Schematic representation of the experimental protocol. Cells were cultured in medium supplemented with TRITC-labelled NPs for the time defined in the panel, washed, and characterized by flow cytometry (FACS). (E) Uptake of TRITC-labelled RA⁺NPs (10 μg/mL) in UCB CD34⁺ cells as quantified by FACS. (F) Percentage of cells labelled with fluorescent RA⁺NPs along cell culture. After TRITC-NP incubation (4 h) cells were washed with PBS to remove non-internalized RA⁺NPs and cultured in complete media for additional 4 h, 3 days or 6 days and finally characterized by flow cytometry. (G) Representative confocal imaging of 4 h internalization of TRITC-labelled RA⁺NPs (red) in UCB CD34⁺ cells stained with the membrane marker PKH67 green and nuclear staining DAPI. Scale bar is 5 μm. (H) Differentiation profile in UCB CD34⁺ cells after treatment with soluble RA or RA⁺NPs. UCB CD34⁺ cells were incubated in medium containing soluble RA or RA⁺NPs (1 μg/mL) for 4 h. Then, cells were washed three times with PBS to remove NPs and irradiated with a blue laser (405 nm, 40 mW, 60 s). After 3 days in culture, cells were stained for CD34 and CD38 markers and differentiation analyzed by flow cytometry in terms of percentage of cells positive for CD34/CD38 inside the live cells gate. In A, B, C, E, F and H, results are expressed as Mean ± SEM (n = 3). Statistical analyses were performed by one-way ANOVA (A,B) or two-way ANOVA (C,H) followed by the Holm-Sidak posttest. *P < 0.05, **P < 0.01, ***P < 0.001 and ****P < 0.0001.

points, cells were collected, and the percentage of NP-loaded cells was evaluated by flow cytometry (Fig. 6F, Supplementary Fig. 4C and D). Our results showed that the percentage of NP-labelled cells decreased to approximately 20% after 6 days in culture. This decrease can be due to nanoparticle efflux mediated by ABC transporters that are highly expressed in HSCs [46]. These results suggest that these RA⁺NPs have an activation time-window of up to 6 days in HSCs, however, for best results, activation should be within the first 2 days of cell infusion *in vivo* (~70% of the cells loaded).

Next, we evaluated the differentiation capacity effect of RA⁺NP in UCB CD34⁺ cells. Cells were incubated in medium with soluble RA (0.11 µg/mL), empty NPs (1 µg/mL) or RA⁺NPs (1 µg/mL of RA⁺NPs containing 0.11 µg/mL of RA) for 4 h. We have used less RA⁺NPs than previous assays to have more sensitivity to measure RA impact in cell differentiation. Then, cells were washed with PBS to remove NPs and irradiated with a blue laser (405 nm, 40 mW, 60 s). After 3 days in culture, cells were stained for CD34 and CD38 markers and differentiation analyzed by flow cytometry (Fig. 6H and Supplementary Fig. 4E). Cells treated with empty NPs had residual levels of differentiation, similarly to the non-treated condition (Supplementary Figs. 4E and 4E.1). Cells treated with RA⁺NPs and activated by light showed the most significant increase in CD38 staining when compared to all other conditions. These results showed that we can induce a differentiation program in these cells triggered by RA-release from NP by light. Our results also showed that differentiated cells have no significant alterations in the expression of CD34 epitope. These results are in line with previous observations, where soluble RA induced CD38 expression in normal hematopoietic progenitor cells [47].

2.5. *In vivo* engraftment of hematopoietic mouse progenitor cells transfected with RA⁺NPs

Since we have shown that polymeric light-triggerable NPs could be efficiently loaded in human HSCs and remotely activated without toxic effects while maintaining their functionality, we decided to further explore their potential use in a non-disease model of hematopoietic mouse progenitors transplantation. We have used the positivity in terms of expression of the stem cell marker c-Kit (a cell surface protein tyrosine kinase which interacts with its cognate ligand, stem cell factor (SCF), to regulate HSC self-renewal) and lineage negative sorting (lineage negative means that the HSCs do not express a panel of protein surface markers present on mature blood lineage cells) to select bulk HSPCs cells for transplantation. Live BM hematopoietic Lineage⁻c-Kit⁺ cells (here referenced only as c-Kit⁺ cells) were isolated from CD45.1 donor mice, incubated with RA⁺NP (1 µg/mL) and transplanted into lethally irradiated CD45.2 recipients together with supporting CD45.2 BM cells. Recipients were then photoactivated with blue light in the calvaria at 24 h and 48 h after transplantation (RA⁺NPs + light) (Fig. 7A). Additional control groups included mice receiving c-Kit⁺ progenitors without NPs and photoactivation (c-Kit⁺ only), c-Kit⁺ progenitors with empty NPs but receiving photoactivation (empty NPs + light) and c-Kit⁺ progenitors with RA⁺NPs but without photoactivation (RA⁺NPs). These controls were found necessary to evaluate: (i) the effect of the components of the NP formulation, without RA, (ii) the effect of the radiation in the cells, and (iii) the effect of RA that may leach from the NP formulation when the formulation is not photoactivated. We tracked the recipients every 4 weeks for 24 weeks and did not observe significant differences in peripheral blood (PB) reconstitution (Fig. 7B). No significant differences were detected in B cells, T cells, monocytes and granulocytes arising from CD45.1 (Supplementary Figs. 5 and 6) or CD45.2 cells (Supplementary Figs. 5 and 7) between the different groups. At 24 weeks, the BM was analyzed, and we could detect a trend of increased total cells (Fig. 7C), Lineage⁻, c-Kit⁺ (Fig. 7E) and LKS stem (Lin⁻, c-Kit⁺, Sca-1⁺) and progenitor cells (MPPs) arising from CD45.1 cells (Fig. 7F and Supplementary Fig. 5A). Interestingly, no differences were detected in the CD45.2 compartment, suggesting that photoactivated RA⁺NPs

enhance the engraftment of carrier cells without affecting surrounding hematopoiesis (Fig. 7E and F).

Our results showing that RA favor hematopoietic progenitor engraftment at the BM is in agreement with a previous study showing that low concentrations (5 µM) of RA promoted engraftment and maintenance of healthy dormant-HSCs (dHSCs), a quiescent long-term reconstitution population [13]. When LKS cells were cultured with RA for 72 h and transplanted into recipient mice there were no differences in terms of the presence of donor-derived cells in PB. After secondary recipient transplantation there was ~6-fold increase in donor-derived cells in PB, indicating the presence of higher percentage of LT-HSCs in the BM of the first recipient-mouse that received RA-treated cells [13]. Our results are in agreement with this engraftment effect of RA but our approach may be more beneficial as we only need 1 h incubation with RA⁺NPs, avoiding the 72 h exogenous RA treatment that may be detrimental for clinical application. To the best of our knowledge, this is the first study documenting the effect of RA in long-term hematopoietic reconstitution using a *in situ* activation approach without any exogenous priming or genetic conditioning of the transplanted cells.

Our approach compares favorably to other nanomedicine strategies reported previously. One elegant approach used HSC-bound multilamellar lipid nanoparticles carrying a GSK-3β inhibitor that were able to reconstitute recipient animals with rapid kinetics after BM transplants without affecting multilineage differentiation potential [48]. This study reported a 5-fold increase in the number of donor-derived cells in the BM after 2 weeks, and no differences in the percentage of donor-derived cells in the spleen, after 12 weeks. As the results of this study had an endpoint at 12 weeks it is unclear the potential for long-term reconstitution of this cell-modulation strategy. Our approach has the advantage of having a good early BM reconstitution capacity that is reflected in the peripheral blood compartment, but most importantly, there is more than a 10-fold increase in retention of donor cells in the BM at 24 weeks, when compared with controls. The fact that our NPs are hidden inside the cell and are activated *in situ* within the BM seems to enable an efficient long-term engraftment. Future experiments should address what is the mechanism behind our engraftment results but it has already been demonstrated *in vitro* that RA inhibits proliferation through induction of cell-cycle arrest [49,50], maintains dHSCs and preserves critical properties of HSCs under stress conditions (pIC, LPS, 5-FU) *in vivo* [13]. This is associated with decreased Cdk6 levels, expression of Hoxb4 (key transcription factor), decreased protein synthesis, and reactive oxygen species (ROS) generation as well as low Myc protein levels [13]. Furthermore, the cell-specific expression of the various RAR receptors can also be the reason for the documented bipolar effect of RA. Transcriptomics data has shown a low expression of Rar-α in the dHSC compartment [13]. Future studies should explore the exact mechanism of the distinct effect of RA signaling in dormant mouse and human HSCs versus more mature cell types and acute myeloid leukemia LSCs.

3. Conclusions

Our results show that light-sensitive RA⁺NPs can induce a differentiation program in LSCs towards a monocyte/macrophage lineage with impact in the overall number of leukemia cells at different BM sites and not only in the photoactivated BM. We have shown *in vitro* an increase in anti-tumoral M1 macrophages when RA⁺NPs were used instead of soluble RA. This is due to modulation of gene expression by RA, namely through RIG1 signaling, that is potentiated by the co-adjuvant induction of OASL by NPs. Our *in vivo* results show that mouse AML cells transfected with RA⁺NPs home at the BM after transplantation in a AML mouse model and the activation of the NPs by a laser make the delivery cells with systemic anti-leukemic effects. We further show that non-disease mouse hematopoietic progenitor cells transfected with RA⁺NPs home at the BM and the activation of the NPs by a laser enhanced the delivery cell engraftment at the BM. This is the first time that a RA intervention is done *in situ* at the BM, with impact in long-term

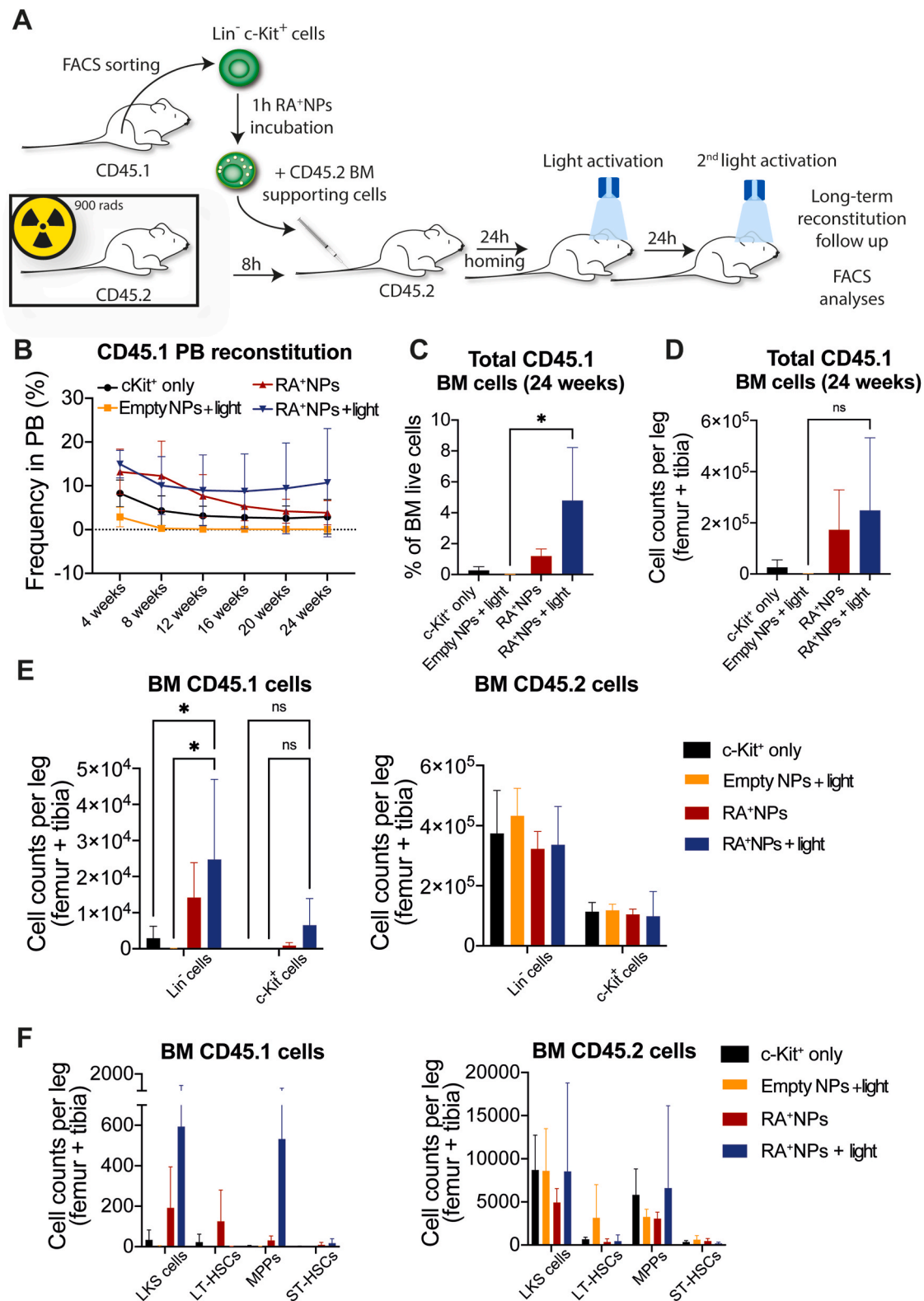


Fig. 7. c-Kit⁺ progenitor cells transfected with RA⁺NPs have long-term reconstitution. (A) Schematic representation of the experimental protocol. c-Kit⁺ progenitor cells isolated from CD45.1 donor mice were transfected with or without NPs (empty and RA⁺NPs) (1 μ g/mL) in XVIVO15 medium for 1 h. Recipient CD45.2 mice were lethally irradiated and then transplanted with 200,000 supporting CD45.2 BM cells and 63,000 CD45.1 c-Kit⁺ progenitors (previously incubated with or without NPs) by intravenous injection (tail vein). Finally, mice were irradiated in the calvaria with a blue laser for 10 min at 24 and 48 h post-transplantation for photoactivation of the NPs. (B, C) Analysis of (B) frequency and (C) absolute CD45.1 BM cell numbers at 24 weeks post-transplantation. (D, E) Quantification of (D) Lineage⁻ (Lin⁻) and c-Kit⁺ cells and (E) LKS progenitors within the CD45.1 (left) and CD45.2 (right) compartments. In B, C, D, E and F, results are expressed as Mean \pm SEM (n = 3–4 mice per group). Statistical analysis was performed using two-way ANOVA (B, E, F) and Kruskal-Wallis multiple comparison test (C and D). Only significant comparisons (*P < 0.05) are shown for clarity.

hematopoietic reconstitution of transplanted cells. The present research reports a blue laser inducible NP that was designed for initial proof of concept regarding the modulation of leukemic cell niches in the bone marrow. Recent studies have explored blue laser approaches to trigger *in vivo* the presentation of bioligands with spatial temporal control to regulate cell adhesion, inflammation, and vascularization of biomaterials [51] and to detect protease activity at sites of disease [52]. However, the *in vivo* applications of this light trigger are limited, as the optical properties of biological tissue cause attenuation and scattering of light rays, reducing their penetration depth. The recent advances in developing NPs activated by near-infrared light [53,54] may provide a better option for enhancing light penetration in tissues. As alternative, the use of injectable hydrogels [55] or medical devices for the local delivery of RA in the bone marrow, as shown for other organs [56], might be also considered for investigation in the near future.

4. Experimental section/methods

4.1. Animals

All animals received humane care according to the criteria outlined by the ARRIVE (Animal Research: Reporting of *In Vivo* Experiments) and FELASA (Federation of European Laboratory Animal Science Associations) guidelines (EU Directive 2010/63/EU). Experimental procedures carried out in Portugal were approved by the i3S Animal Ethics Committee (DD_2019_15) and Direção-Geral de Alimentação e Veterinária (DGAV). Experimental procedures carried out in the UK were in accordance with Home Office regulations, following ICL AWERB approval. Animals were housed under specific pathogen-free conditions, in a temperature and light-controlled environment, with free access to standard rodent chow (Teklad Global 14% Protein Rodent Maintenance Diet containing 175 mg/kg iron, Harlan Laboratories) and water. Mice were obtained from the i3S and ICL animal facilities and from Charles River (France). Blood was obtained by tail vein bleeds of up to 20 μ L.

4.2. Human samples

Human umbilical cord blood samples were obtained from donors who signed an informed consent form, in compliance with Portuguese legislation. The collection methods were authorized and carried out in accordance with the approved guidelines and regulations by the ethical committee of Maternity Daniel de Matos (Coimbra) and Hospital Infante D. Pedro (Aveiro). The samples were stored in sterile bags containing 35 mL of citrate-phosphate-dextrose anticoagulant solution. CD34⁺ cells were isolated from mononuclear cells, obtained from UCB samples after Ficoll/Histopaque-1077 Hybri Max (Sigma-Aldrich, Missouri, USA) density gradient separation. CD34⁺ cells were positively selected (2 times) using the mini-MACS immunomagnetic separation system (Miltenyi Biotec, Bergisch Gladbach, Germany), according to the manufacturer's recommendations.

4.3. NP preparations, characterization, and *in vitro* photo-disassembly

NP preparation has been described in detail in a previous publication [6]. Briefly, light-inducible polymeric NPs, are composed of poly(ethyleneimine) (PEI) derivatized with 4,5-dimethoxy-2-nitrobenzyl chloroformate (DMNC), a light-sensitive photochrome. The degree of substitution (DS) of DMNC in PEI was confirmed by ¹H NMR (DS = 10%). PEI facilitates the cellular internalization of NPs and their subsequent escape from endosomes [23,57], and DMNC responds rapidly to light and its degradation products are relatively non-cytotoxic [58]. In a dark vial, RA (1.2 mg, 34 μ L of 35 mg/mL in DMSO) was dissolved in a Milli-Q water solution (5620 μ L) of PEI-DMNC (10 mg, 66.7 μ L of 150 mg/mL in DMSO) under stirring. Then, dextran sulfate (DS) (2 mg, 40 μ L of 50 mg/mL in water) was added to form NPs by electrostatic (PEI:DS) and hydrophobic (DMNC:DMNC) interactions and to encapsulate the

RA. Next, NPs were stabilized with zinc sulfate (240 μ L, 1 M) [23,59] and the final volume of the formulation (6 mL) was stirred for additional 30 min. The unloaded RA was removed by centrifugation (12,000 g–3 min) and finally a powder of RA⁺NPs was obtained after freeze-drying using 5% mannitol as cryoprotectant. The size and zeta potential of the NPs were obtained by dynamic light scattering (DLS) (ZetaPALS analyser, Brookhaven Instruments Corp.). For particle size, an amount of NPs powder (2 mg) was resuspended in water (1 mL), sonicated for 10 s, and diluted to 50 μ g/mL (2 mL) in a DLS cuvette. After an equilibration time of 5 min, NPs size was obtained as the mean of 5 measurements runs. Data were analyzed with the software developed by the manufacturer using a distribution analysis. The reported mean diameter of the NPs was calculated based on number distribution. For zeta potential, the NPs solution was measured in the presence of 1 mM of KCl and the results were calculated from the electrophoretic mobility based on the Helmholtz-Smoluchowski relationship. NPs can be photo-disassembled by UV light or using a conventional blue laser (405 nm, 80 mW). The response of the NPs to a blue laser is mediated by DMNC coupled to PEI, as NPs without DMNC do not respond to the laser. The responsiveness of the NPs to UV light was measured by DLS and obtained by determination of the NP count after irradiation respective to the non-irradiated sample. Details on the conditions necessary to trigger intracellular NP disassembly can be found in Ref. [6].

4.4. Drug loading and encapsulation efficiency measurements

To determine RA encapsulation efficiency and RA loading capacity of the NPs, the concentration of RA was determined by analytical reverse-phase HPLC on a Shimadzu Prominence-I LC-2030C 3D, using a XBridge C18 3.5 μ m 4.6 \times 250 mm column (Waters). The mobile phase consisted of a mixture of acetonitrile (ACN) (HPLC grade, Acros) and water containing 0.08% of trifluoroacetic acid (TFA) (Merck). The mobile phase started with a flow rate of 1 mL/min at 80:20% of H₂O-TFA/ACN-TFA for 2 min, then changed to 100% ACN-TFA over 13 min, followed by 3 min at 100% ACN-TFA and finally changed to initial ratio 80:20% over 7 min. RA was monitored at 350 nm. The amount of entrapped RA in the NPs was determined by resuspension of lyophilized RA⁺NPs in DMSO, injected into the HPLC, and accessed using a calibration curve of RA (0–700 μ g/mL), $y = 16170x$. The percentage of encapsulation efficiency (1) and drug loading capacity (2) was calculated by using the following formula:

- (1) Encapsulation efficiency (%) = $\frac{\text{Weight of the RA in RA}^+\text{NPs}}{\text{Weight of the feeding RA}} \times 100$.
- (2) Drug loading capacity (%) = $\frac{\text{Weight of the RA found in the lyophilized NPs}}{\text{Weight of lyophilized NPs}} \times 100$.

4.5. Drug release studies

[³H]RA solution in DMSO was used for the preparation of NPs, using a 1:10 ratio of labelled to unlabelled RA (1 nCi/ μ g RA). The initial RA cargo in the NPs was quantified using 2/3 of the original NP suspension (1 mg/mL). To quantify the controlled release of the RA, a 10 μ g/mL suspension of [³H]RA-NPs was prepared and irradiated with a blue laser (405 nm, 80 mW/cm²). For each timepoint (0s, 60s, 180s, 300s, 600s) the NP suspension was centrifuged at 14,000 g for 3 min, the supernatant collected and mixed with liquid scintillation fluid (1 mL; Packard Ultima Gold) and the scintillations counted in a TriCarb 2900 TR Scintillation analyser (PerkinElmer). The amount of RA was determined by the linear regression equation $y = 1.3985x$ ($R^2 = 0.9947$).

4.6. RA⁺NPs internalization by MLL-AF9 blasts and differentiation

YFP and mTmG MLL-AF9 AML cells were prepared as described [60]. MLL-AF9 cells were maintained in complete medium [RPMI-1640 supplemented with 10% FBS (heat inactivated), 1% Pen/Strep, 1%

L-glutamine+10 ng/mL SCF and IL-6 and 6 ng/mL IL-3] until experiments. YFP MLL-AF9 cells were incubated in serum-free RPMI-1640 with RA⁺NPs (10 µg/mL) for 4 h. Then, cells were washed three times with PBS to remove NPs not internalized, activated or not by blue laser (405 nm, 80 mW, 5 min), and cultured in complete medium for additional 3 days. Alternatively, YFP MLL-AF9 were cultured in complete medium for 3 days having soluble RA (1.1 µg/mL). The differentiation at 72 h post treatment was evaluated by flow cytometry: GMPs (Ly6G⁺CD11b⁻), neutrophil (Ly6G⁺CD11b⁺) and macrophage (Ly6G⁻CD11b⁺F4/80⁺) differentiation markers. The macrophage cells were also characterized for their polarization in type 1 (MHC II⁺CD206⁻) and type 2 (MHC II⁻CD206⁺). The flow cytometry analyses comprised the following steps: live=> single cells=> ly6g/cd11b => cd206/MHC II. Percentages of positive cells were calculated based in the isotype controls (1% of overlap with the isotype scatter plot). FlowJo was used for data analysis.

4.7. Evaluation of RA⁺NPs endolysosomal escape

mTmG MLL-AF9 cells were incubated for 4 h in RPMI medium without serum with RA⁺NPs (10 µg/mL) or 50 µM hydroxychloroquine (HQ). After 4 h, the cells were washed in PBS and left in culture for additional 24 h in RPMI 1640 supplemented with 10% FBS (heat inactivated), 1% Pen/Strep, 1% L-glutamine, 10 ng/mL SCF and IL-6 and 6 ng/mL IL-3. After 24 h the cells were collected, centrifuged, and resuspended in 100 µL of medium and immobilized into a glass slide by cytospin. The cells were then fixed in 4% PFA for 10 min, washed in PBS and permeabilized using 0.1% Triton for 10 min. The cells were blocked in a solution of 1% BSA and 0.3 M glycine (45 min) and left over-night at 4 °C with the primary antibody for galectin 9 (1:100; catalog number: 137,901, clone 108A2, Biologend). After 3 washes (5 min each) in PBS the cells were incubated for 1 h at room temperature with the secondary antibody (Alexa 488- Donkey anti-rat, 1:500). Following 3 washes in PBS the cells were incubated with DAPI (2 µg/mL) for 5 min and mounted with Vectashield. The cells were visualized in a Zeiss 7100 confocal microscope. For each condition 3–4 fields were acquired. For each field the number of cells with galectin 9 foci (green dots) was counted and normalized for the total number of nuclei (DAPI staining) of the corresponding field.

4.8. mRNA expression analyses in MLL-AF9 YFP cells transfected with RA⁺NPs or cultured in the presence of soluble RA

YFP MLL-AF9 cells were incubated in serum-free RPMI-1640 with RA⁺NPs (1 µg/mL) for 4 h. Then, cells were washed three times with PBS to remove not internalized NPs, activated or not by blue laser (405 nm, 80 mW) during 5 min, and cultured in complete medium for additional 3 days. Alternatively, YFP MLL-AF9 were cultured in complete medium for 3 days having soluble RA (0.11 µg/mL). RNA extraction was performed after 24 and 72 h. Each RNA sample was diluted to the same concentration (14 ng/µL). Reverse transcriptase enzyme [qScript cDNA super mix (Quanta BioSciences); 1 µL] was added to 4 µL of each RNA sample to obtain cDNA. Each cDNA sample was pre-amplified with PreAmp Master Mix enzyme (Fluidigm) according to the enzyme manufacturer for 12 cycles. After Exonuclease to remove unincorporated primers [Exonuclease I (New England Biolabs)] the samples were diluted 10x in TE buffer. For each sample a Pre-Mix was prepared with SsoFast Eva Green Supermix (BioRad) and 20x DNA binding dye sample reagent (Fluidigm). Each sample (5 µL) was pipetted into the respective inlet of a Fluidigm® 48.48 Gene expression IFC. For each assay (gene) a mix of 12 µL was individually prepared: 6 µL of 2x Assay loading reagent (Fluidigm), 5.4 µL of TE buffer, 1.2 µL from a stock of 50 µM each mixed forward and reverse primers. Each assay (5 µL) was pipetted into their respective assay inlets on the chip. The assay and sample mixes were loaded with the corresponding Load mix script of the MX controller (HD Biomark). After loading the IFC qRT-PCR was carried out on BioMark

HD™, accordingly to the cycling parameters recommended by Fluidigm® for 48.48 Gene expression IFC. Data were collected with Data Collection Software and were analyzed using Fluidigm® Real Time PCR Analysis v2.1 software. Genes with melting curves displaying more of one peak (amplification of non-specific products) were not included in the analysis. The data were normalized for the reference gene Actb and fold was calculated versus the respective non-treated cells.

4.9. Evaluation of OASL and RIG1 protein levels

NB4 cells (acute promyelocytic leukemia cell line) were incubated in serum-free RPMI-1640 with RA⁺NPs (1 µg/mL) for 4 h. Then, cells were washed three times with PBS to remove non-internalized NPs, activated by blue laser (405 nm, 80 mW) during 5 min, and cultured in complete medium. Alternatively, NB4 were cultured in complete medium with soluble RA (0.11 µg/mL). After 72 h the cells were collected, centrifuged, and resuspended in 100 µL of medium and immobilized into a glass slide by cytospin. The cells were fixed in 4% PFA for 10 min, washed in PBS and permeabilized using 0.1% Triton for 10 min. The cells were blocked in a solution of 1% BSA, followed by a 2 h incubation at RT with anti-RIG-I/DDX58 antibody (1:50; catalog number: ab238254, Abcam). After 3 washes (5 min each) in PBS the cells were incubated for 1 h at room temperature with the secondary antibody (Alexa 647- Donkey anti-goat, 1:500). This was followed by an overnight incubation with anti-OASL primary antibody (1:100; catalog number: PA5-81946, Thermo Fisher Scientific). After 3 washes (5 min each) in PBS the cells were incubated for 1 h at room temperature with the secondary antibody (Alexa 488- Donkey anti-rabbit, 1:500). Nuclei were counterstained with DAPI (2 µg/mL) for 5 min and mounted with Vectashield. The cells were visualized in a Zeiss 710 confocal microscope. For each condition 3–4 fields were acquired. For each field, a ROI (region of interest) was created around each cell, the fluorescence intensity was measured and normalized by the area of each cell.

4.10. Intravital microscopy to monitor cell activity inside the calvaria BM niche

First mTmG MLLAF9 blasts were injected in healthy mice to induce disease infiltration. After 11 days YFP MLL-AF9 blasts previously loaded with RA⁺NPs or empty NPs were injected. One or two days later, after confirming the homing of YFP blasts to the same niche as mTmG blasts by intravital microscopy, the nanoparticles were activated by exposing the mouse calvaria to the blue laser for 5 min (10 s “ON” + 5 s “OFF”). This activation was repeated the following day. Three days after the last activation, the progression of the disease and MLL-AF9 activity were monitored inside the niche by time-lapse image acquisition. In the end of the acquisitions, mice were sacrificed, and BM was collected from the calvaria and long bones and analyzed by flow cytometry.

4.11. Tail vein administration of MLL-AF9 YFP cells carrying empty NPs or RA⁺NPs

After the BM homing (day 1) of YFP MLL-AF9 cells transfected with empty NPs or RA⁺ NPs, the formulations were remotely activated by irradiating the mouse calvaria with a blue laser (5 min, 405 nm, 80 mW) on the following two days. On the fifth day after YFP MLL-AF9 administration, mice were sacrificed and BM from the calvaria and long bones isolated for flow cytometry analysis.

4.12. RA⁺NPs internalization, cytotoxicity and light activation of UCB CD34⁺

UCB CD34⁺ cells were maintained until experiments in complete medium [X-VIVO 15 (Lonza)+ 50 ng/mL of Flt-3+ 50 ng/mL SCF]. Uptake of TRITC-labelled RA⁺NPs (10 µg/mL) by UCB CD34⁺ cells was determined by FACS. Cells were cultured in medium supplemented with

NPs, washed and characterized by flow cytometry. UCB CD34⁺ cells were transfected with RA⁺NPs in X-VIVO 15 media for 4 h, washed with PBS to remove non-internalized RA⁺NPs and cultured in complete media for additional 4 h, 3 days and 6 days. After each incubation time cells were washed, and NP dilution evaluated by flow cytometry.

4.13. Differentiation profile of UCB CD34⁺ cells after transfection with RA⁺NPs

Cells were transfected with RA⁺NPs and empty NPs (without RA) (1 µg/mL, 4 h), washed with PBS, suspended in complete medium and then irradiated with a blue laser at time 4 h, or 72 h or 144 h. As a control condition, soluble RA was added to cells at the same time of laser activation of each group. In all groups, the differentiation was evaluated 3 days after activation by flow cytometry (CD34/CD38 staining). FITC mouse anti-human CD38 (clone: HIT2, BD Biosciences) and APC anti-human CD34 (clone: AC136, Miltenyi Biotec) at a dilution of 1:20 were used.

4.14. Transplantation of c-Kit⁺ progenitors and long-term reconstitution

Lineage⁻ c-Kit⁺ cells were isolated from CD45.1 donor mice for transplantation into CD45.2 recipient mice. CD45.1 donor mice were euthanized, and BM cells were obtained from femurs, tibias and iliac bones and depleted of red blood cells through incubation with red blood cell lysis buffer (Biolegend). BM cells were then incubated with biotin-conjugated anti-mouse lineage cocktail (CD3_e (145-2C11), CD4 (GK1.5), CD8a (53-6.7), CD11b (M1/70), CD45R/B220 (RA3-6B2), Ly-6G/Ly-6C (Gr-1) (RB6-8C5) and TER-119 (TER-119), all from Biolegend) (1:20) for 30 min at 4 °C, subsequently incubated with streptavidin magnetic beads (New England BioLabs) for 30 min at 4 °C and passed through LD magnetic columns (Miltenyi Biotec) for depletion of lineage positive cells. Lineage depleted BM cells were then incubated with biotinylated anti-mouse lineage cocktail (1:50) and APC/Cyanine7 anti-mouse CD117 (c-Kit) (2B8) antibody (1:100, Biolegend) for 30 min at 4 °C and subsequently stained with APC Streptavidin (1:1000, Biolegend) for 15 min at RT. Lineage⁻ c-Kit⁺ cells were sorted using a FACS Aria II (BD Biosciences). Sorted CD45.1 c-Kit⁺ progenitors were incubated with or without RA⁺NPs (1 µg/mL) in X-VIVO 15 medium (Lonza) for 1 h at 37 °C, 5% CO₂ in a water jacketed cell incubator (Forma Scientific). Recipient CD45.2 mice were lethally irradiated (~900 rads) using a Gammacell 1000 irradiator (Best Theratronics) 8 h before transplantation with 200,000 supporting CD45.2 BM cells and 63,000 CD45.1 c-Kit⁺ progenitors (previously incubated with or without NPs) in 120 µL PBS by intravenous injection (tail vein). Finally, mice were shaved and irradiated in the calvaria with a blue laser for 10 min at 24 and 48 h post-transplantation for photoactivation of the NPs.

Ethics approval

All animal work was done according to ARRIVE (Animal Research: Reporting of In Vivo Experiments) and FELASA (Federation of European Laboratory Animal Science Associations) guidelines (EU Directive 2010/63/EU). Experimental procedures carried out in Portugal were approved by the i3S Animal Ethics Committee (DD_2019_15) and Direção-Geral de Alimentação e Veterinária (DGAV). Experimental procedures carried out in the UK were in accordance with Home Office regulations, following ICL AWERB approval.

Consent to participate

Cord-blood – human umbilical cord blood samples were obtained from donors, who signed an informed consent form, in compliance with Portuguese legislation. The collection methods were authorized and carried out in accordance with the approved guidelines and regulations by the ethical committee of Maternity Daniel de Matos (Coimbra) and

Hospital Infante D. Pedro (Aveiro).

Consent for publication

Not applicable.

Availability of data and material

Not applicable – all supporting data is included in the manuscript as supplementary materials.

Funding

The authors would like to acknowledge funding from FCT—Fundação para a Ciência e a Tecnologia under project(s): DOI 10.54499/2022.05946.PTDC, UIDB/04539/2020, UIDP/04539/2020 and LA/P/0058/2020; and PRR project HfPT. This study was also supported by research funding from the European Hematology Association (EHA Physician-Scientist Research Grant), Fundação Amélia de Mello and National Blood Foundation to DD.

CRediT authorship contribution statement

Emanuel Quartin: Conceptualization, Investigation, Methodology, Writing – original draft, Writing – review & editing. **Susana Rosa:** Investigation, Methodology, Writing – review & editing. **Sara Gonzalez-Anton:** Investigation, Methodology. **Laura Mosteo Lopez:** Investigation, Methodology. **Vitor Francisco:** Investigation, Methodology. **Del-fim Duarte:** Funding acquisition, Investigation, Methodology, Resources, Writing – original draft, Writing – review & editing. **Cristina Lo Celso:** Funding acquisition, Investigation, Methodology, Resources, Writing – original draft, Writing – review & editing. **Ricardo Pires das Neves:** Conceptualization, Funding acquisition, Investigation, Methodology, Supervision, Writing – original draft, Writing – review & editing. **Lino Ferreira:** Conceptualization, Funding acquisition, Investigation, Methodology, Project administration, Supervision, Writing – original draft, Writing – review & editing.

Declaration of competing interest

Authors declare no competing interests.

Acknowledgements

Authors would like to acknowledge funding agencies and colleagues from the Biomaterials and Stem Cell Based Therapeutics Lab for helpful discussions and suggestions.

Appendix A. Supplementary data

Supplementary data to this article can be found online at <https://doi.org/10.1016/j.bioactmat.2023.12.017>.

References

- [1] H. Dohner, D.J. Weisdorf, C.D. Bloomfield, *N. Engl. J. Med.* 373 (2015) 1136–1152.
- [2] H. Kantarjian, T. Kadia, C. DiNardo, N. Daver, G. Borthakur, E. Jabbour, G. Garcia-Manero, M. Konopleva, F. Ravandi, *Blood Cancer J.* 11 (2021) 41.
- [3] R. Ferreira, J. Napoli, T. Enver, L. Bernardino, L. Ferreira, *Nat. Commun.* 11 (2020) 4265.
- [4] F. Lo-Coco, G. Avvisati, M. Vignetti, C. Thiede, S.M. Orlando, S. Iacobelli, F. Ferrara, P. Fazi, L. Cicconi, E. Di Bona, G. Specchia, S. Sica, M. Divona, A. Levis, W. Fiedler, E. Cerqui, M. Breccia, G. Fioritoni, H.R. Salih, M. Cazzola, L. Melillo, A. M. Carella, C.H. Brandts, E. Morra, M. von Lilienfeld-Toal, B. Hertenstein, M. Wattad, M. Lubbert, M. Hanel, N. Schmitz, H. Link, M.G. Kropp, A. Rambaldi, G. La Nasa, M. Luppi, F. Ciceri, O. Finizio, A. Venditti, F. Fabbiano, K. Dohner, M. Sauer, A. Ganser, S. Amadori, F. Mandelli, H. Dohner, G. Ehninger, R.F. Schlenk, U. Platzbecker, d.A. Gruppo Italiano Malattie Ematologiche, G. German-Austrian

- acute myeloid leukemia study and L. Study alliance, *N. Engl. J. Med.* 369 (2013) 111–121.
- [5] C.W. Duan, J. Shi, J. Chen, B. Wang, Y.H. Yu, X. Qin, X.C. Zhou, Y.J. Cai, Z.Q. Li, F. Zhang, M.Z. Yin, Y. Tao, J.Q. Mi, L.H. Li, T. Enver, G.Q. Chen, D.L. Hong, *Cancer Cell* 25 (2014) 778–793.
- [6] C. Boto, E. Quartin, Y. Cai, A. Martin-Lorenzo, M.B.G. Cenador, S. Pinto, R. Gupta, T. Enver, I. Sanchez-Garcia, D. Hong, R. Pires das Neves, L. Ferreira, *Nat. Commun.* 8 (2017) 15204.
- [7] G.B. Adams, R.P. Martin, I.R. Alley, K.T. Chabner, K.S. Cohen, L.M. Calvi, H. M. Kronenberg, D.T. Scadden, *Nat. Biotechnol.* 25 (2007) 238–243.
- [8] J. Hoggatt, P. Singh, J. Sampath, L.M. Pelus, *Blood* 113 (2009) 5444–5455.
- [9] R. Gupta, V. Turati, D. Brian, C. Thrusell, B. Wilbourn, G. May, T. Enver, *Cell Stem Cell* 26 (2020) 527–541, e528.
- [10] E.Z. Szuts, F.I. Harosi, *Arch. Biochem. Biophys.* 287 (1991) 297–304.
- [11] P.D. Fiorella, J.L. Napoli, *J. Biol. Chem.* 269 (1994) 10538–10544.
- [12] G. Ghiatur, S. Yegnasubramanian, B. Perkins, J.L. Gucva, J.M. Gerber, R.J. Jones, *Proc. Natl. Acad. Sci. U.S.A.* 110 (2013) 16121–16126.
- [13] N. Cabezas-Wallscheid, F. Buettner, P. Sommerkamp, D. Klimmeck, L. Ladel, F. B. Thalheimer, D. Pastor-Flores, L.P. Roma, S. Renders, P. Zeisberger, A. Przybylla, K. Schonberger, R. Scognamiglio, S. Altamura, C.M. Florian, M. Fawaz, D. Vonficht, M. Tesio, P. Collier, D. Pavlinic, H. Geiger, T. Schroeder, V. Benes, T.P. Dick, M. A. Rieger, O. Stegle, A. Trumpp, *Cell* 169 (2017) 807–823, e819.
- [14] G.M. Crane, E. Jeffery, S.J. Morrison, *Nat. Rev. Immunol.* 17 (2017) 573–590.
- [15] S. Pinho, P.S. Frenette, *Nat. Rev. Mol. Cell Biol.* 20 (2019) 303–320.
- [16] Y. Morita, H. Ema, H. Nakauchi, *J. Exp. Med.* 207 (2010) 1173–1182.
- [17] I.L. Weissman, J.A. Shizuru, *Blood* 112 (2008) 3543–3553.
- [18] M. Krohn-Grimberghe, M.J. Mitchell, M.J. Schloss, O.F. Khan, G. Courties, P.P. G. Guimaraes, D. Rohde, S. Cremer, P.S. Kowalski, Y. Sun, M. Tan, J. Webster, K. Wang, Y. Iwamoto, S.P. Schmidt, G.R. Wojtkiewicz, R. Nayar, V. Frodermann, M. Hulsmans, A. Chung, F.F. Hoyer, F.K. Swirski, R. Langer, D.G. Anderson, M. Nahrendorf, *Nat. Biomed. Eng.* 4 (2020) 1076–1089.
- [19] A. Swami, M.R. Reagan, P. Basto, Y. Mishima, N. Kamaly, S. Glavey, S. Zhang, M. Moschetta, D. Seevaratnam, Y. Zhang, J. Liu, M. Memarzadeh, J. Wu, S. Manier, J. Shi, N. Bertrand, Z.N. Lu, K. Nagano, R. Baron, A. Sacco, A.M. Roccaro, O. C. Farokhzad, I.M. Ghoobrial, *Proc. Natl. Acad. Sci. U.S.A.* 111 (2014) 10287–10292.
- [20] H. Zong, S. Sen, G. Zhang, C. Mu, Z.F. Albayati, D.G. Gorenstein, X. Liu, M. Ferrari, P.A. Crooks, G.J. Roboz, H. Shen, M.L. Guzman, *Leukemia* 30 (2016) 1582–1586.
- [21] A.M. Dorrance, P. Neviani, G.J. Ferenchak, X. Huang, D. Nicolet, K.S. Maharry, H. G. Ozer, P. Hoellarbauer, J. Khalife, E.B. Hill, M. Yadav, B.N. Bolon, R.J. Lee, L. J. Lee, C.M. Croce, R. Garzon, M.A. Caligiuri, C.D. Bloomfield, G. Marcucci, *Leukemia* 29 (2015) 2143–2153.
- [22] B.M. Barth, I.A.E.S.S. Shanmugavelandy, J.M. Kaiser, D. Crespo-Gonzalez, N. A. DiVittore, C. McGovern, T.M. Goff, N.R. Keasey, J.H. Adair, T.P. Loughran Jr., D. F. Claxton, M. Kester, *ACS Nano* 5 (2011) 5325–5337.
- [23] J. Maia, T. Santos, S. Aday, F. Agasse, L. Cortes, J.O. Malva, L. Bernardino, L. Ferreira, *ACS Nano* 5 (2011) 97–106.
- [24] T. Santos, R. Ferreira, E. Quartin, C. Boto, C. Saraiva, J. Braganca, J. Peca, C. Rodrigues, L. Ferreira, L. Bernardino, *Acta Biomater.* 59 (2017) 293–302.
- [25] T.C. Somerville, M.L. Cleary, *Cancer Cell* 10 (2006) 257–268.
- [26] K. Sakamoto, T. Imamura, M. Yano, H. Yoshida, A. Fujiki, Y. Hirashima, H. Hosoi, *Blood Cancer J.* 4 (2014) e205.
- [27] H. Du Rietz, H. Hedlund, S. Wilhelmson, P. Nordenfelt, A. Wittrup, *Nat. Commun.* 11 (2020) 1809.
- [28] D.J. Mangelsdorf, H.P. Koeffler, C.A. Donaldson, J.W. Pike, M.R. Haussler, *J. Cell Biol.* 98 (1984) 391–398.
- [29] P. Sinha, V.K. Clements, S. Ostrand-Rosenberg, *J. Immunol.* 174 (2005) 636–645.
- [30] X. Yang, W. Feng, R. Wang, F. Yang, L. Wang, S. Chen, Y. Ru, T. Cheng, G. Zheng, *Oncolmunology* 7 (2018) e1412910.
- [31] F.O. Martinez, S. Gordon, M. Locati, A. Mantovani, *J. Immunol.* 177 (2006) 7303–7311.
- [32] R. Guo, M. Lu, F. Cao, G. Wu, F. Gao, H. Pang, Y. Li, Y. Zhang, H. Xing, C. Liang, T. Lyu, C. Du, Y. Li, R. Guo, X. Xie, W. Li, D. Liu, Y. Song, Z. Jiang, *Biomark. Res.* 9 (2021) 15.
- [33] K.L. Anderson, K.A. Smith, H. Perkin, G. Hermanson, C.G. Anderson, D.J. Jolly, R. A. Maki, B.E. Torbett, *Blood* 94 (1999) 2310–2318.
- [34] P.Y. Lee, J.X. Wang, E. Parisini, C.C. Dascher, P.A. Nigrovic, *J. Leukoc. Biol.* 94 (2013) 585–594.
- [35] C. Chen, R. Wang, W. Feng, F. Yang, L. Wang, X. Yang, L. Ren, G. Zheng, *Ann. Transl. Med.* 9 (2021) 266.
- [36] Z.J. Xu, Y. Gu, C.Z. Wang, Y. Jin, X.M. Wen, J.C. Ma, L.J. Tang, Z.W. Mao, J. Qian, J. Lin, *Oncolmunology* 9 (2020) 1683347.
- [37] Y. Que, H. Li, L. Lin, X. Zhu, M. Xiao, Y. Wang, L. Zhu, D. Li, *Front. Immunol.* 12 (2021) 653030.
- [38] F.O. Martinez, S. Gordon, *F1000Prime Rep.* 6 (2014) 13.
- [39] K.E. Miari, M.L. Guzman, H. Wheadon, M.T.S. Williams, *Front. Cell Dev. Biol.* 9 (2021) 692800.
- [40] Q. Zhao, J. Tao, Q. Zhu, P.M. Jia, A.X. Dou, X. Li, F. Cheng, S. Waxman, G.Q. Chen, S.J. Chen, M. Lanotte, Z. Chen, J.H. Tong, *Leukemia* 18 (2004) 285–292.
- [41] E. Nguyen, G. Gausdal, J. Varennes, F. Pendino, M. Lanotte, S.O. Doskeland, E. Segal-Bendirdjian, *Mol. Pharmacol.* 83 (2013) 1057–1065.
- [42] S.F. Wu, L. Xia, X.D. Shi, Y.J. Dai, W.N. Zhang, J.M. Zhao, W. Zhang, X.Q. Weng, J. Lu, H.Y. Le, S.C. Tao, J. Zhu, Z. Chen, Y.Y. Wang, S. Chen, *Proc. Natl. Acad. Sci. U.S.A.* 117 (2020) 14395–14404.
- [43] C. Kyogoku, B. Smiljanovic, J.R. Grun, R. Biesen, U. Schulte-Wrede, T. Haupt, F. Hiepe, T. Alexander, A. Radbruch, A. Grutzkau, *PLoS One* 8 (2013) e83776.
- [44] S. Eskildsen, J. Justesen, M.H. Schierup, R. Hartmann, *Nucleic Acids Res.* 31 (2003) 3166–3173.
- [45] C. Lo Celso, H.E. Fleming, J.W. Wu, C.X. Zhao, S. Miale-Lye, J. Fujisaki, D. Cote, D. W. Rowe, C.P. Lin, D.T. Scadden, *Nature* 457 (2009) 92–96.
- [46] M.H. Raaijmakers, *Leukemia* 21 (2007) 2094–2102.
- [47] E. Prus, E. Fibach, *Leuk. Lymphoma* 44 (2003) 691–698.
- [48] M.T. Stephan, J.J. Moon, S.H. Um, A. Bershteyn, D.J. Irvine, *Nat. Med.* 16 (2010) 1035–1041.
- [49] S.E. Jacobsen, C. Fahlman, H.K. Blomhoff, C. Okkenhaug, L.S. Rusten, E. B. Smeland, *J. Exp. Med.* 179 (1994) 1665–1670.
- [50] L.E. Purton, I.D. Bernstein, S.J. Collins, *Blood* 94 (1999) 483–495.
- [51] T.T. Lee, J.R. Garcia, J.I. Paez, A. Singh, E.A. Phelps, S. Weis, Z. Shafiq, A. Shekaran, A. Del Campo, A.J. Garcia, *Nat. Mater.* 14 (2015) 352–360.
- [52] J.S. Dudani, P.K. Jain, G.A. Kwong, K.R. Stevens, S.N. Bhatia, *ACS Nano* 9 (2015) 11708–11717.
- [53] V. Shanmugam, S. Selvakumar, C.S. Yeh, *Chem. Soc. Rev.* 43 (2014) 6254–6287.
- [54] V. Francisco, M. Lino, L. Ferreira, *J. Nanobiotechnol.* 17 (2019) 97.
- [55] N. Olov, S. Bagheri-Khoulenjani, H. Mirzadeh, *Prog. Biomater.* 11 (2022) 113–135.
- [56] S. Huang, D. Lei, Q. Yang, Y. Yang, C. Jiang, H. Shi, B. Qian, Q. Long, W. Chen, Y. Chen, L. Zhu, W. Yang, L. Wang, W. Hai, Q. Zhao, Z. You, X. Ye, *Nat. Med.* 27 (2021) 480–490.
- [57] O. Boussif, F. Lezoualc’h, M.A. Zanta, M.D. Mergny, D. Scherman, B. Demeneix, J. P. Behr, *Proc. Natl. Acad. Sci. U.S.A.* 92 (1995) 7297–7301.
- [58] T. Dvir, M.R. Banghart, B.P. Timko, R. Langer, D.S. Kohane, *Nano Lett.* 10 (2010) 250–254.
- [59] W. Tiyaboonchai, J. Woiszwillo, C.R. Middaugh, *J. Pharmaceut. Sci.* 90 (2001) 902–914.
- [60] D. Duarte, E.D. Hawkins, O. Akinduro, H. Ang, K. De Filippo, I.Y. Kong, M. Haltalli, N. Ruivo, L. Straszowski, S.J. Vervoort, C. McLean, T.S. Weber, R. Khorshed, C. Pirillo, A. Wei, S.K. Ramasamy, A.P. Kusumbe, K. Duffy, R.H. Adams, L. E. Purton, L.M. Carlin, C. Lo Celso, *Cell Stem Cell* 22 (2018) 64–77 e66.